

Pushbroom imaging spectrometer with high spectroscopic data fidelity: experimental demonstration

Pantazis Mouroulis, MEMBER SPIE
Michael M. McKerns*
Jet Propulsion Laboratory
California Institute of Technology
Pasadena, CA 91109

Abstract. Experimental results are described from a pushbroom imaging spectrometer module demonstrating very low spectral and spatial distortion (a few percent of a pixel) and similarly small variation in spectral response function with field position. These spectrometer properties significantly facilitate the extraction of accurate spectroscopic information. The spectrometer can achieve high performance despite relaxed tolerances in fabrication and alignment. A quick and effective alignment method is described that permits the spectrometer to approximate its design performance. The implications of the results for the calibration techniques of pushbroom imaging spectrometers are also discussed.
© 2000 Society of Photo-Optical Instrumentation Engineers. [S0091-3286(00)03103-2]

Subject terms: optical design; imaging spectroscopy; hyperspectral imaging; remote sensing; distortion; spectral calibration.

Paper 990112 received Mar. 16, 1999; revised manuscript received Aug. 4, 1999; accepted for publication Aug. 5, 1999.

1 Introduction

Pushbroom imaging spectrometers are a desirable form for Earth observations from space, since they can achieve a higher signal-to-noise ratio than their whiskbroom counterparts. At the same time, they carry the penalty of increased calibration difficulty. While in a whiskbroom spectrometer all pixels have their spectra recorded by a single linear photodetector array, for a pushbroom spectrometer with 700 to 1000 spatial pixels there are effectively that many different linear arrays or spectrometers in need of calibration.

The need for accurate calibration of Earth-looking hyperspectral sensors has been recently recognized.¹ The location of the peak of the spectral response function (SRF) and its half-width (as well as shape) must be known to within a small fraction of the nominal pixel bandwidth, typically less than a few percent. Translated into pushbroom spectrometer terms, this requirement means that uncalibrated distortion along the spatial direction (called *smile*) as well as the spatial variation of the optical PSF must be kept to a minimum, typically a small fraction of a pixel. Smile is defined here as the deviation from straightness of the monochromatic image of the slit (Fig. 1).

Even if errors induced by the above factors can be corrected by calibration, minimizing the errors will decrease substantially the computational complexity of data reduction. Another practical reason for insisting on field independence of the SRF peak location has to do with calibration. Measurement of the peak location of the SRF for a pushbroom sensor is complicated because it requires an accurately calibrated monochromator. Such calibration is pos-

sible only over a small part of the monochromator slit (essentially a point), because available monochromators suffer from considerable smile, thus causing an uncertainty in the absolute wavelength. Translation of the monochromator up and down the slit of the test spectrometer is a laborious experimental procedure of doubtful accuracy. Therefore, it is easier to rely on an independent smile measurement from which the SRF peak locations can be inferred. Ideally, such measurement would show lack of smile, hence allowing the same SRF peak location to be used independently of spatial position. Even if the SRF shape is not spatially invariant, its relative shape can be measured with much greater ease than the absolute peak location. Hence simple methods of reducing as well as measuring smile are of importance.

In addition to the above-noted restrictions on the SRF variation, it is also desirable to reduce the distortion along the spectral direction (called *keystone*). Keystone is the variation of slit magnification with wavelength, but it is measured here as an absolute length value (or fraction of a pixel—see Fig. 1). This error means that the amount of mixing of the spectra from spatially adjacent pixels will vary with wavelength. This affects the recovered spectrum of pixels located close to sharp boundaries in the image, or of targets that are less than a few pixels large. A general keystone tolerance is difficult to give, as the effect of the error will depend (at least) on the form of the spectra and the optical point spread function (PSF). A simulation using two different types of vegetation and an ideal PSF revealed that the keystone error must be controlled to a small fraction of a pixel, although a more relaxed tolerance of less than about 0.1 pixel can apply here.²

This paper contains the description and performance tests of an imaging spectrometer module, which was designed and built in order to verify that small distortion can be achieved in practice, and in order to develop the tech-

*Present address: Department of Physics, University of Alabama Birmingham, Birmingham, AL 35294.

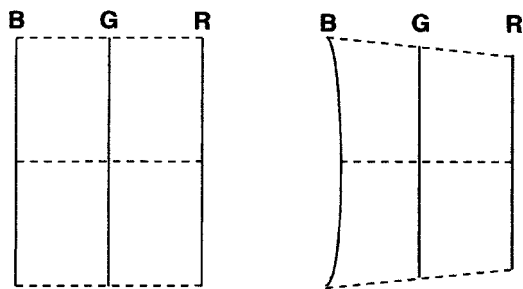


Fig. 1 Schematic of the spectrum produced by a pushbroom imaging spectrometer. On the left, the lines for blue(B), green(G), and red(R) are all straight, parallel, and aligned with the detector array. Also, the magnification is independent of wavelength. On the right, the B column exhibits smile, which is measured as the sag of the B line. Also, the magnification depends on wavelength, causing the G and R lines to be shorter than the B line. The amount of keystone is given by the difference in length between the B and R lines.

niques for doing so. It is shown that high performance can be achieved with a simple and compact optical design. The prototype approaches 2% in smile and ≈8% keystone (limited by measurement accuracy). It may be worth repeating that these percentages refer to the pixel size and not to the total field size, as is more common in optical design. To our knowledge, this is the first time that a system is demonstrated to achieve these low levels of error in practice. For example, an evaluation of commercial spectrometers as well as a specially designed unit³ similar to the one described here revealed smile and keystone errors on the order of one pixel. We are concerned here with a further reduction of these errors by one to two orders of magnitude.

2 Spectrometer Design

The spectrometer is of the Offner form,⁴⁻⁶ which has been used previously in space applications.^{7,8} The full potential of the Offner form is now being realized thanks to recent developments in convex-grating fabrication by electron-beam (EB) lithography.⁹ Alternative Offner spectrometer forms utilizing prisms have been proposed,¹⁰ but a grating-based all-reflective system is simpler and more robust if an efficient and low-scattering convex grating can be had. Several design forms have been described that achieve in theory low levels of distortion.¹¹ A preliminary report on the spectrometer described here has also appeared.¹² In this paper, we expand the preliminary results of Ref. 12 to encompass both smile and keystone, provide full experimental results of the spectrometer performance, and discuss in detail the alignment technique that enables the high level of performance to be easily achieved in practice.

Table 1 Spectrometer specifications.

f number	2.8
Pixel size (spatial×spectral)	12×13.7μm ²
Spatial pixels	754
Spectral pixels	185 (0.4–1 μm, 480 available)
Slit magnification	–1
Spectral sampling	3.2 nm

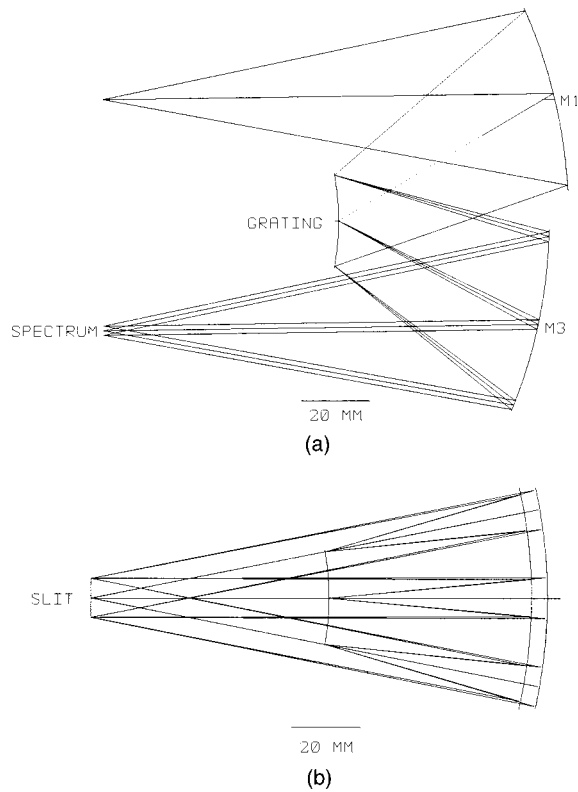


Fig. 2 (a) Schematic of the spectrometer in the y-z plane. The slit is perpendicular to the plane of the paper. The long-wavelength end of the spectrum is at the top. (b) Schematic of the spectrometer in the x-z plane. The slit and its image are coincident in this projection.

2.1 Specification and Prescription Data

The basic specifications are given in Table 1. The spectrometer was originally designed as an f/2.8 system with a ≈1-cm slit (nominal 1024 spatial pixels of 10-μm size). A compromise CID focal-plane array (CIDTEC 3710D) was used, mostly for budgetary reasons. Pixel dimensions are shown in Table 1.

The design schematic is shown in Fig. 2(a) (y-z view) and Fig. 2(b) (x-z view). The design prescription is given in Table 2. The slit is displaced by 33.24 mm from the system axis. All mirrors are spherical and with a common axis of symmetry. Primary and tertiary have also been made concentric, which facilitates alignment. No tilts or decenters are used in the design. All design and evaluation was done using ZEMAX.¹³

Table 2 Prescription data.

Surface	Type	Radius (mm)	Thickness (mm)	Glass
OBJ		∞	136.0869	
1	Standard	–135.839	67.22123	Mirror
STO	Diff. grating	–68.415	61.48648	Mirror
3	Standard	–130.1043	–130.21365	Mirror
IMA		∞		

Table 3 Grating characteristics.

Order	+1
Pitch	16.2 μm
Clear aperture	25 mm
Sag	1.1 mm

Grating characteristics are given in Table 3. The grating is a single-blaze design, with the blaze peak at around 575 nm. Detailed efficiency tests were not performed on the grating, but several similar gratings have been made consistently with $>87\%$ peak first-order relative efficiency.⁹ In any case, the efficiency itself is of no importance for this paper. A rather more critical characteristic of the grating is that the blaze angle remains constant across its extent (relative to the local surface normal). This characteristic, enabled by the EB fabrication technique, combines with the small variation of incidence angles that is inherent in the design to produce a grating that has approximately constant diffraction efficiency across its entire aperture. This means that the grating can be modeled in a simple manner, without the need for introducing complicated wavelength-dependent apodization factors.

2.2 Design Performance

Since the design has nearly diffraction-limited performance, we must use diffraction-based metrics. The various performance parameters are summarized in Table 4. The smile is measured as the maximum difference in the x coordinate of the PSF centroids. Other parameters are self-explanatory. This performance is achieved without the need for aberration correction in the grating.

3 Fabrication and Alignment

3.1 Tolerancing and Component Tests

Tolerance analysis of the initial design revealed that two of the three curvatures could be fitted to manufacturer's testplates (primary, grating). The curvature of the tertiary and the spacings were then used as variables to reoptimize performance. This resulted in an increase in smile from practically zero to the above-quoted 2% of pixel size. The tolerance of the tertiary radius was set at 0.1%. Other mirrors were toleranced at 2 fringes power and 0.5 fringe irregularity. Those tolerances have a negligible effect on performance (change in merit function by a few percent, using the final distance as compensator).

The primary and tertiary had less than 0.1-wave p-v error over the beam footprint. An interferogram of the grating was very hard to obtain in the zero order because of the minuscule amount of light remaining in that order—the interferometer could not acquire the fringes for automatic analysis. However, sufficient fringe contrast was obtained to ascertain the surface quality visually. Again, the surface irregularity was estimated to be <0.1 wave. An interferogram in the first order was easy to obtain, but it shows considerable off-axis astigmatism as expected. The zero-order (rather than the first-order) result is representative of what the grating substrate contributes to the overall Offner error, since the astigmatism is at least partly compensated by the rest of the optics.

3.2 Optics Alignment

The following optics alignment method has been developed. The complete method is specific to Offner spectrometers with either a combined primary-tertiary or separate but concentric primary and tertiary (both spherical). However, several of the steps apply in more general cases as well. It is noted that the Offner design often allows the mirrors to be concentric without any serious penalty and that the use of tilts or decenters in the design is rarely justified. Thus the designer should strive to achieve concentricity, which will permit easier alignment of the primary and tertiary and may allow them to be easily manufactured as a monolithic block.

First, the primary and tertiary were coarsely positioned. Fine positioning was achieved interferometrically. Using a fast focusing lens at the interferometer, both mirrors are illuminated simultaneously and the zero-fringe position is determined for the portion of the wavefront returned by each mirror. When less than half a fringe is seen on both halves, the mirrors are concentric to that accuracy. This adjustment is done manually, and its accuracy is more than adequate.

With the primary and tertiary thus fixed, and with the interferometer focus at their common center of curvature, the entire spectrometer is translated laterally by the amount dictated by the prescription in order to bring the interferometer focus to the middle of the hypothetical slit. At that point, the actual slit may be positioned so as to let the interferometer beam pass without any vignetting. If the slit location is not coincident with the common center of curvature (in terms of its z -coordinate value), then translation along z will also be needed. Generally, the tolerance for slit defocus is not tight, so the nominal accuracy of a manual micrometer-driven stage suffices for this last adjustment.

Table 4 Spectrometer design performance. The range of values given in some columns indicates worst to best case as a function of field location. MTF (tan.) is along the spectral direction, and MTF (sag.) along the spatial direction, at the Nyquist frequency of the detector array.

λ (nm)	Strehl	PSF energy in pixel (%)	MTF (tan.)	MTF (sag.)	Smile (% of pixel size)	Keystone (% of pixel size)
400	0.43–0.84	>94	0.86–0.93	0.93–0.95	1.8	
1000	0.85–0.90	>90	0.83–0.86	0.84–0.85	1.5	1

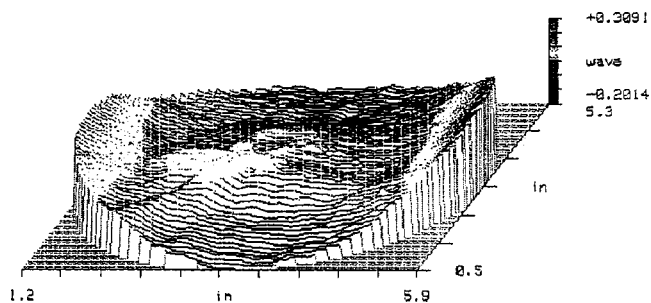


Fig. 3 Measured wavefront from the spectrometer at 633 nm and for the center of the slit. The main aberration is astigmatism. The middle bump is due to mirror figure. The p-v error is 0.51λ .

The interferometer focus is now at the middle of the slit location. The grating is then coarsely positioned. A return concave mirror is used to test the entire Offner in double pass. First, the grating is clocked (rotated about z) in an approximate way by looking at the image of the diffracted orders and making those nominally horizontal. The correct order is identified for returning with the mirror.

A series of interferograms of the complete system in double pass are then taken while adjusting the grating position and tilt. The aim is to reduce the wavefront error to the minimum possible, depending on individual mirror surface quality. The grating position thus determined is not the final, but only an intermediate one. It has been found that the grating tilt and decenter control the amount of coma, while the z location controls the astigmatism. Thus the grating alignment is best achieved by first minimizing coma using grating tilt or decenter adjustment only, and then by minimizing astigmatism using the z translation.

The minimum peak-to-valley (p-v) error that was achieved was 0.24 wave and was consistent with the mirror quality and individual mirror interferograms. The residual amount of coma and astigmatism was down to about 0.1 wave.

At this point, the optical design software is used in order to simulate the minimum-wavefront-error configuration for a point at the center of the slit. This is done by merely varying the z position of the grating through the software. This minimum-error location is not the final one, because the spectrometer has been optimized for minimum distortion as well as for balanced image quality over all field points. The position of the grating determined by the software is then compared with the final design prescription. The grating is finally translated along the z axis by the difference between the two locations (or better, by observing the amount of astigmatism induced and arriving at the desired value according to the prescription data). In the case at hand, the required motion was in the range of 30 to 40 μm , resulting in an increase in astigmatism to 0.4 wave, which was close to the design value for the f number used. The necessity of determining the minimum-wavefront-error position arises from the fact that a given amount of astigmatism can be induced by a forward as well as backward movement of the grating from that position. The above procedure removes this ambiguity.

The resulting interferogram is shown in Fig. 3. All wavefront errors in this section refer to an f number of 3.2 (rather than the minimum design f number of 2.8), which

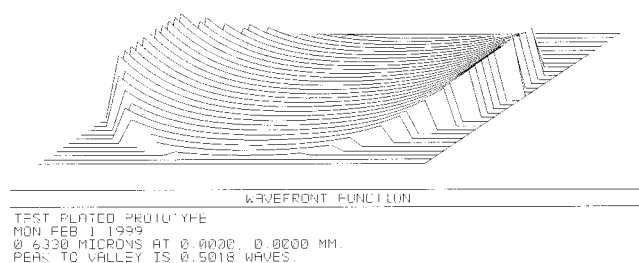


Fig. 4 Predicted wavefront at 633 nm and $f/3.2$ for the center of the slit, using the design prescription data. The p-v error is 0.5λ .

was determined by the interferometer. The p-v error is 0.51 wave. The corresponding wavefront generated by ZEMAX for these conditions is shown in Fig. 4 as having an almost purely astigmatic p-v error of 0.5 wave, and can be compared with the wavefront shown in Fig. 3. The middle bump seen in Fig. 3 is due to mirror surface irregularity.

Next, the slit was aligned to vertical. This was accomplished by translating the entire spectrometer vertically and ensuring that the focused spot from the interferometer passed through the slit unvignetted during the entire travel. Two more interferograms were taken at the edges of the slit. The resulting wavefronts differed by ≈ 0.1 wave p-v from the expected values. These two interferograms confirmed that the spectrometer has better image quality (less astigmatism) at the edges of the slit than at the center, as was expected from the design data.

The focal plane was then aligned by observing the image of the slit illuminated with various spectral lamps, as discussed in Sec. 4.2 below. The optics alignment was then complete except for precise grating rotational alignment (clocking). It is imperative that this adjustment be achieved without disturbing the previous alignment, and the equipment needs to be designed so as to permit that. Otherwise, a movement of the grating necessitates realignment using the interferometer.

This alignment method has been found quick and repeatable. It was possible to realign the entire spectrometer (with the exception of the focal plane) within a few hours, starting from near-arbitrary mirror positions. The method allows us to achieve a specified wavefront error rather than a minimum error, and thus determine the minimum distortion position without actually measuring the distortion.

4 Tests

4.1 Dispersion Test

The extra spectral pixels of the camera permitted recording of the zero order, which provided a convenient reference point. ZEMAX was used to determine the expected distance between the zero order and various spectral lines. This distance was then converted into pixels, and gave a predicted pixel location for any one wavelength. Using an argon spectral lamp, the positions of five spectral lines observed in the range 690 to 850 nm were compared with their expected values. The agreement between observed and expected values was within a half pixel.

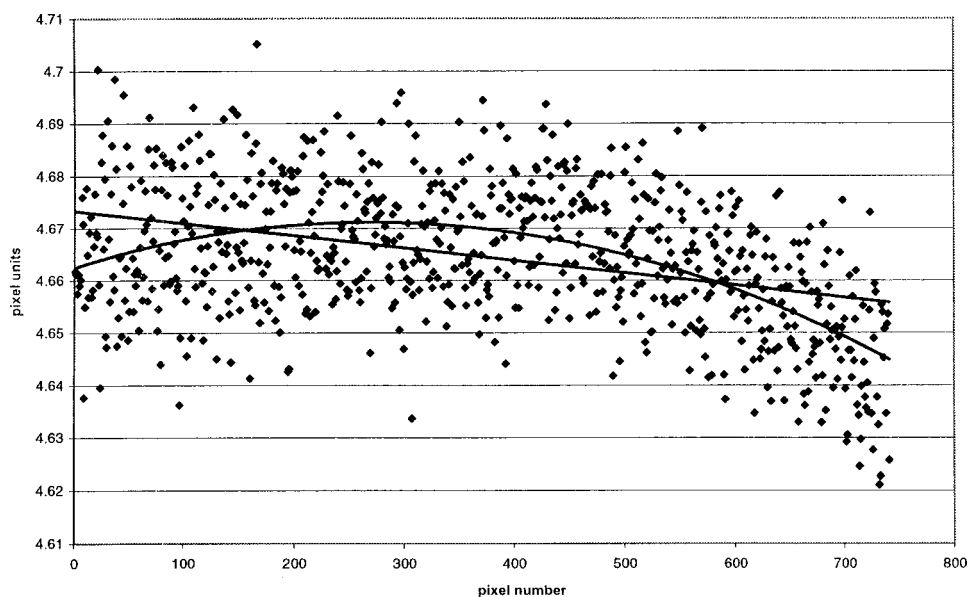


Fig. 5 Measurement of smile for the 546.1-nm Hg line. The abscissa is the column number, and the ordinate is the location of the centroid for each column, given in fractional pixel units. The fitted lines are first- and second-degree least-squares curves.

4.2 Smile Measurement

The method for measuring smile is simple. A slit is imaged on the focal plane and illuminated by various spectral lamps at specified wavelengths. The spectral lamp was vertical, and a lens was used to image the lamp onto the slit at a nominal 1:1 magnification. With this arrangement, it was found that the measured smile and even line rotation depended on the illumination (focus, lamp tilt, etc.), implying a less than uniform illumination of the slit, even across its width. A diffuser was then inserted near the lens, about equidistant from the slit and the lamp. This was found to eliminate the dependence on the illumination and made the measurement possible. However, the light level was such that only a few strong lines could be recorded.

A high-quality slit is needed. Ours was fabricated by EB lithography. Commercially purchased ruled slits were too irregular or not sufficiently straight. The slit used was 2 pixels wide. It was also found that only isolated spectral lines could be used reliably. In other words, at least two noise pixels (preferably three or four) are needed before the next spectral line starts.

The monochromatic image of the slit was recorded by the array (along a row). A simple centroiding calculation was then performed along each column, over approximately ten pixels, spanning the image of the line. The resulting centroids (approximately 750, the same in number as the spatial pixels of the array) were then plotted with appropriate trendlines. A straight nonhorizontal line indicates net rotation. A curved line indicates smile or similar distortion. This method is used also to align the array rotationally with respect to the slit.

Figures 5 and 6 show the results achieved for two different spectral lines: the 546.1-nm Hg line and the 912.3-nm Ar line. Taking the smile to be the difference between the two fitted lines (quadratic and linear), we determine a smile of $\approx 2\%$ of pixel, consistent with the design value. But the agreement is not perfect, because according

to the design data, the smile is not supposed to turn into a frown at the long-wavelength end. Two more lines were recorded, a 435-nm Hg and a 760-nm Kr. Those lines also showed a smile level of less than 2%, but the net slope was not always consistent, varying between +1% and -1%. The reason for the discrepancy between measurement and theory is not obvious. It is possibly caused by the mirror figure error and residual small misalignment from the design positions, or it may represent a limitation of the measurement method and equipment. Of course one should keep in mind that we are attempting to measure extremely small values of smile and rotation (1% of a pixel is 0.13 μm , across a field of 750 pixels or 9 mm).

The results of Figs. 5 and 6 represent the average of four frames in order to reduce noise. Background frame subtraction was tried but was found not to be useful, as it increased the noise. It seemed preferable to shield the stray light as much as possible in a darkened room. Also, pixel sensitivity calibration was not performed. This was not deemed necessary because of the large number of pixels that are involved in the centroiding and the trendline calculation. In any case, the results were found to be independent of the location of the spectral line on the array, and repeated measurements over the same area did not reveal substantial systematic errors.

4.3 Keystone Measurement

Keystone is measured by imaging a pinhole that is illuminated by a nominally white source (a tungsten-halogen bulb, which was imaged at $\approx 1:1$ on the pinhole). This results in a spectrum that forms a line along a column of the focal plane. Centroiding can be performed in a way similar to that described in the previous section, but in the orthogonal direction. Fitted trend lines can then be compared for tilt or curvature when the pinhole is located at various positions along the slit. The following conditions were needed for a successful measurement.

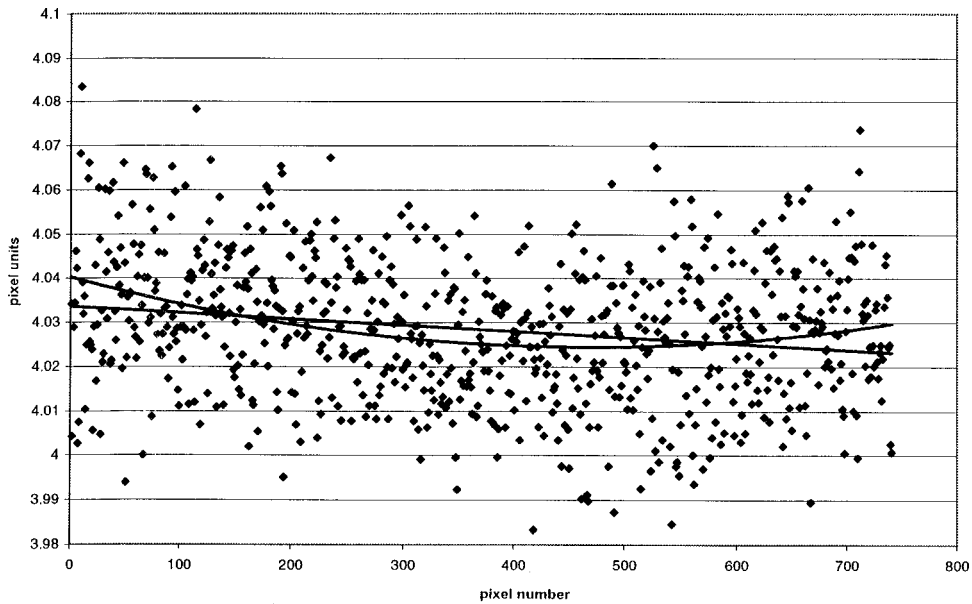


Fig. 6 Measurement of smile for the 912.3-nm Ar line.

1. A flattening spectral filter (CVI EQ-2×2) was found useful. This filter is specifically tailored to equalize the combined response of a CCD and a tungsten source. Use of the filter increases the number of usable pixels by effectively increasing the dynamic range of the camera.
2. The optimum size of the pinhole was found to be at or below the diffraction limit of the system. A small pinhole eliminates any errors caused by the pinhole shape as well as the illumination. The penalty is reduced light level and increased noise, but it is somewhat ameliorated by the fact that no diffuser is needed if the pinhole is so small.
3. The last few pixels at the blue and IR ends of the spectrum cause unreliable results because of the very low signal level. Only the central 150 pixels out of the 180 total spectral pixels were counted; hence the keystone from one end of the spectrum to the other could be expected to be greater by $\approx 20\%$ of the measured value.
4. A fourteen-frame average was taken within approximately 2 s. The resulting reduction in scatter was significant.

The results are shown in Figs. 7 and 8. Figure 7 shows the spectra obtained for four approximately equispaced pin-

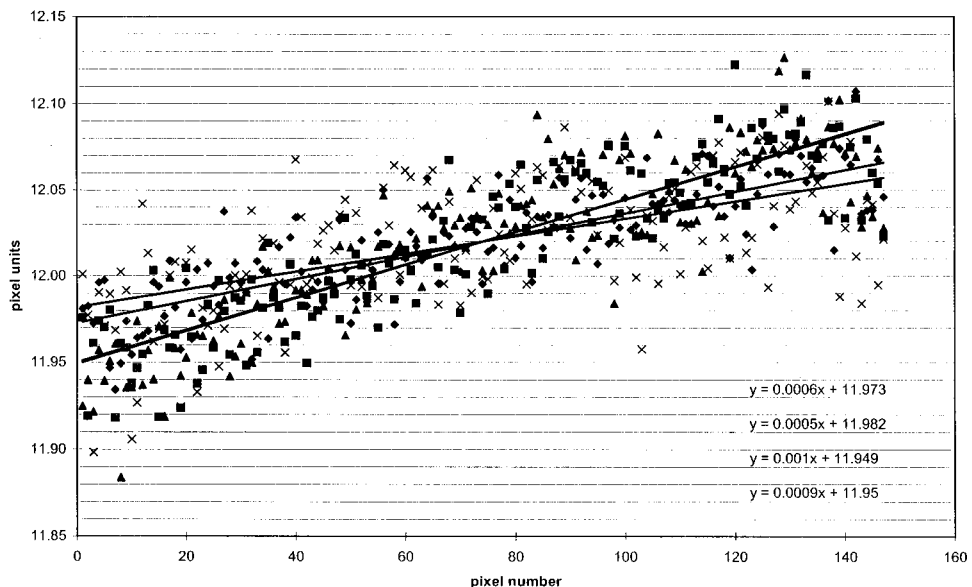


Fig. 7 Spectrum orientation for four different locations along the slit. The average overall tilt of the interpolated lines represents imperfect grating clocking (rotational) alignment. The difference between the lines is indicative of keystone.

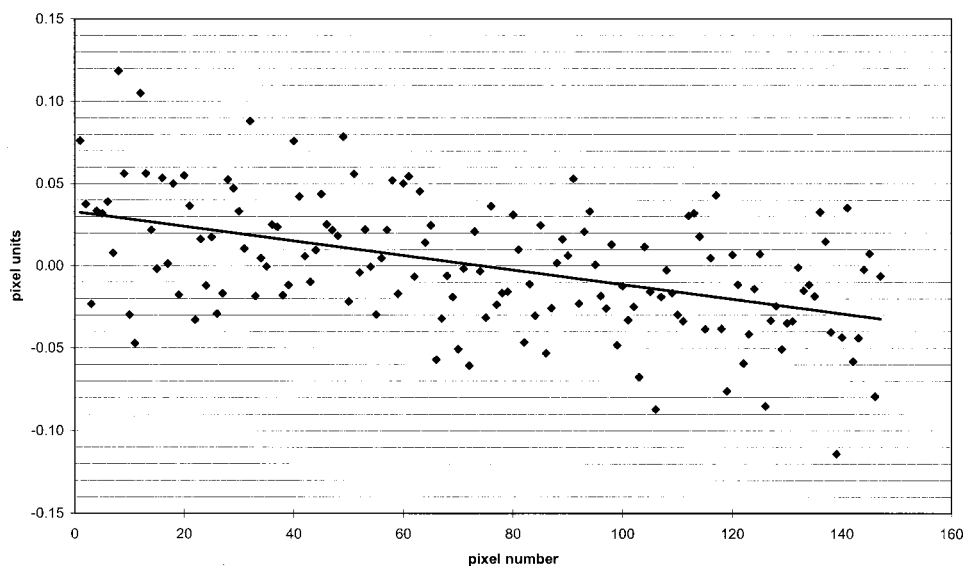


Fig. 8 Net keystone error, obtained as the maximum difference between any two data sets of Fig. 7.

hole locations spanning the entire slit. The figure shows that the clocking of the grating is not the best possible, since there is an average rotation of 0.10 to 0.12 pixel from end to end. Two of the four trendlines are practically identical, but the other two show significant difference.

The precision of the grating clocking is limited by the keystone error. Figure 8 shows the net keystone as the maximum difference between any two data sets from Fig. 7. This is net keystone in the sense that if one of the two data sets is perfectly oriented along the array, the other will show the indicated amount of slope. This way of displaying the data removes the effect of the imperfect grating clocking. Figure 8 shows a net keystone error of just under 7%, which can be extrapolated to $\approx 8.4\%$ in order to include the previously excluded pixels at the ends of the spectrum.

According to the design, the keystone error is symmetric about the middle of the slit, so it should be measured as the difference between the spectra corresponding to the top and bottom of the slit (see also Fig. 1). However, the maximum slope difference between the various trendlines of Fig. 7 does not occur between the two ends of the slit, but between an intermediate position and one end. This discrepancy between design and experimental data cannot be fully explained by residual mirror figure or misalignment errors, and we conclude that the experimental technique is partly responsible. It should be appreciated that when one is trying to measure the lack of an effect, as is the case for both smile and keystone, the accuracy of the experimental apparatus and method will necessarily always be the limiting factor. We believe that the keystone measurements were ultimately limited by stray light, since we achieved a consistent reduction of the measured values with improved shielding. A better baffle and light shield design could be implemented in a field or flight instrument, but our prototype was limited by the use of standard laboratory optical mounts. Stray light may have been more detrimental in this experiment because the imaging light level was lower than it was during the smile measurement. Also, the detector response at the two ends of the spectrum is very low. Thus

stray light of middle wavelengths will have a disproportionate effect if it is incident on pixels that record imaging light of either short or long wavelengths. This effect was largely absent from the smile measurement, since only the strongest lines of the spectral lamps were used there. It can also be avoided in a flight instrument by the use of a linear variable bandpass filter over the focal plane.¹⁴

5 Estimation of the SRF Variation

The SRF of a pixel is normally measured by varying the input wavelength while recording the response of a specific pixel under test.¹⁵ This results in the image of the slit moving along the focal plane from one end of the pixel to the other. The procedure can be described as a convolution of the slit image with the pixel response. The slit image is itself a convolution of the slit (a rectangle function) with the optical line spread function (LSF). For the convolution to be valid, we need to assume that the LSF is invariant over the limited range of wavelengths that excite any one pixel, a condition that is sufficiently satisfied here. Even though the pixel response can be nonuniform,¹⁶ our aim here is not to calibrate the spectrometer as if it were a flight instrument, but merely to show whether there is any variation in SRF caused by the optical design itself. Hence we have chosen to compute the SRF through the above convolution process by taking the pixel response function to be another rect function of equal width to the slit.

From the interferometric data obtained during alignment of the spectrometer, we can determine the actual spectrometer LSF and use that in place of design data. From the three interferometer images that were obtained, we chose the two that give the maximum difference (worst case). The corresponding LSFs are then convolved with the rect functions as above.

Figure 9 compares the SRF computed using the design LSF data with that computed through the measured LSF for the middle of the slit (which gives the worst LSF and widest SRF). It can be seen that the difference is very small.

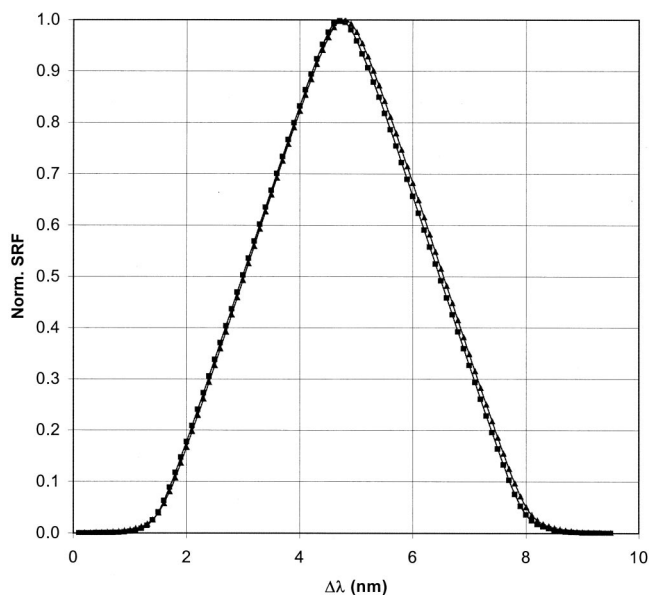


Fig. 9 Experimentally derived (squares) and design SRF (triangles) for the center of the slit and 633-nm wavelength. Both curves refer to the test f number of 3.2.

The experimental and design computed SRFs for the edge of the slit are practically identical and hence not shown here.

For the purposes of this paper, we are concerned with the maximum SRF variation with field position, rather than the absolute SRF shape or width. In this sense, both design and experimental data predict a half-width variation of the SRF of less than 3% for the 633-nm wavelength and $f/3.2$ aperture. But the maximum variation occurs at the short-wavelength end, where the aberrations are more significant. The close agreement shown in Fig. 9 allows us to use design data in order to calculate this maximum variation. The result is shown in Fig. 10, for the maximum spectrometer aperture, $f/2.8$. It can be seen that the two curves are of slightly different shape, and hence their difference is not easily characterized through the change in half-width alone. If we take the latter as sufficient description, we may note that it is less than 5%, and thus would provide approximately the same data accuracy as the smile of 2%.¹ In any case, the difference between the two SRFs is sufficiently small to be detectable only with very accurate calibration techniques.

6 Conclusions

The experimental results have demonstrated a pushbroom sensor with very small amounts of smile ($\approx 2\%$ of pixel size) and keystone ($< 10\%$ of pixel size), and good SRF uniformity, within a few percent half-width variation. The Offner spectrometer can achieve these low levels of smile and keystone with comfortable fabrication tolerances. A quick and reliable alignment method has been developed. A flight instrument with these characteristics would achieve unprecedented spectroscopic data fidelity from a pushbroom sensor.

Techniques for measuring smile and keystone to small fractions of a pixel were demonstrated. The smile measurement was more accurate than the keystone, due to its higher

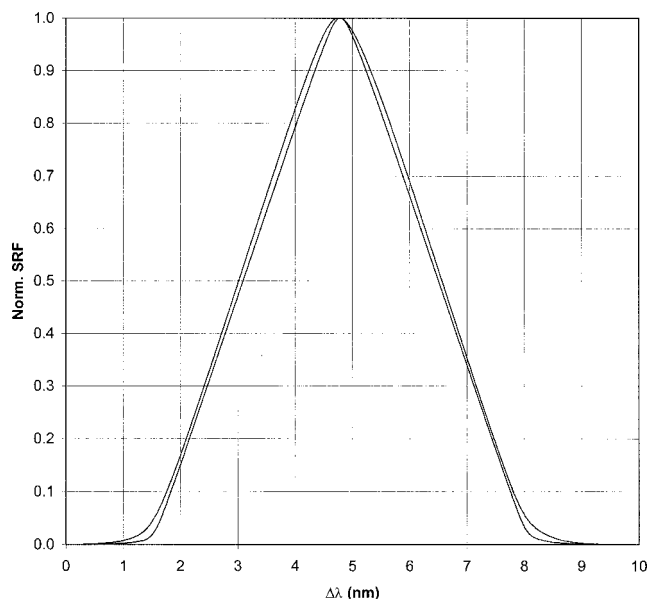


Fig. 10 SRFs for 400 nm and $f/2.8$ obtained from design data. The outer curve is the SRF for the middle of the field (worst LSF), and the inner curve is for the field location that gives the best LSF (approximately 85% of full field). The difference between these two curves represents the maximum SRF variation with field expected from the spectrometer.

and more uniform light level, as well as the larger number of pixels involved in the calculation. The discrepancy between design and experimental values is similar to the measured smile. This discrepancy could be partly caused by residual misalignment or mirror figure errors and partly by measurement inaccuracy. The discrepancy between design and measured keystone values is greater than that for smile. The greater part of the measured keystone of $\approx 8.4\%$ is probably due to measurement limitations rather than fabrication and alignment residuals.

Although it may be possible to develop alternative, more accurate methods for measuring smile and keystone, the methods described here are simple and have the advantage of utilizing the focal plane for which the spectrometer was designed. Therefore, they can also provide the basis for an onboard calibration system that would serve to ensure accurate calibration of a spectrometer throughout the lifetime of a mission. They would also be sufficiently accurate for the planned pushbroom Offner sensors by NASA and other agencies, insofar as one can ascertain the expected level of performance of such sensors from current design data.

Referring to the calibration problems mentioned in the Introduction, the following spectral calibration steps for a pushbroom spectrometer would seem reasonable, based on the current results:

1. Obtain the SRF of a single row of pixels as accurately as possible. This would include knowledge of the absolute location of the peak of the SRF to the specified accuracy.
2. Perform independent smile measurements. Such measurements may be more accurate if an array with smaller pixel size than the flight focal plane array can

be used, but this is not necessary unless one needs even greater accuracy than demonstrated here.

3. Accept that the knowledge of the SRF peak location will be limited in accuracy by the measured smile, or use the measured smile to predict the peak location of the SRF if the smile measurement accuracy can be relied upon.
4. Calibrate other rows for SRF bandwidth only. This does not require knowledge of absolute wavelength with high accuracy.

Acknowledgments

This research was performed at the Jet Propulsion Laboratory, California Institute of Technology, under a contract with the National Aeronautics and Space Administration. We thank Paul Maker, Dan Wilson, and Rich Muller of the JPL Microdevices Laboratory for providing us with the grating and the slits used in this prototype. We also thank David Thomas, Rob Green, Tom Chrien, Jeff Simmonds, and Valerie Duval for technical assistance and the many discussions that culminated in the specifications of this prototype. The support of Jeff Simmonds, Barbara Wilson, and Gregg Vane was crucial for the completion of this project.

References

1. R. O. Green, "Spectral calibration requirement for Earth-looking imaging spectrometers in the solar-reflected spectrum," *Appl. Opt.* **37**, 683–690 (1998).
2. P. Mouroulis, D. A. Thomas, T. G. Chrien, V. Duval, R. O. Green, J. J. Simmonds, and A. H. Vaughan, "Trade studies in multi/hyperspectral imaging systems: final report," NASA Code Y Internal Report, available at <http://nptio.nasa.gov/esto.html> (1998).
3. J. Fisher, M. Baumbach, J. Bowles, J. Grossmann, and J. Antoniadis, "Comparison of low-cost hyperspectral sensors," in *Imaging Spectrometry IV*, M. R. Descour and S. S. Shen, Eds., *Proc. SPIE* **3438**, 23–30 (1998).
4. A. Offner, "Unit power imaging catoptric anastigmat," U.S. Patent No. 3,748,015 (1973).
5. L. Mertz, "Concentric spectrographs," *Appl. Opt.* **16**, 3122–3124 (1977).
6. D. Kwo, G. Lawrence, and M. Chrisp, "Design of a grating spectrometer from a 1 : 1 Offner mirror system," in *Current Developments in Optical Engineering II*, R. E. Fischer and W. J. Smith, Eds., *Proc. SPIE* **818**, 275–278 (1987).
7. F. Reininger, M. Dami, R. Paolinetti, S. Pieri, and S. Falugiani, "Visible infrared mapping spectrometer visible channel (VIMS-V)," in *Instrumentation in Astronomy VIII*, *Proc. SPIE* **2198**, 239–250 (1994).
8. F. Reininger et al., "VIRTIS: visible infrared thermal imaging spectrometer for the Rosetta mission," in *Imaging Spectrometry II*, M. R. Descour and J. M. Mooney, Eds., *Proc. SPIE* **2819**, 66–77 (1996).
9. P. Mouroulis, D. W. Wilson, P. D. Maker, and R. E. Muller, "Convex grating types for concentric imaging spectrometers," *Appl. Opt.* **37**, 7200–7208 (1998).
10. D. R. Lobb, "Imaging spectrometers using concentric optics," in *Imaging Spectrometry III*, *Proc. SPIE* **3118**, 339–347 (1997).
11. P. Mouroulis, "Low-distortion imaging spectrometer designs utilizing convex gratings," in *International Optical Design Conference 1998*, L. R. Gardner and K. P. Thompson, Eds., *Proc. SPIE* **3842**, 594–601 (1998).
12. P. Mouroulis and D. A. Thomas, "Compact, low-distortion imaging spectrometer for remote sensing," in *Imaging Spectrometry IV*, M. R. Descour and S. S. Shen, Eds., *Proc. SPIE* **3438**, 31–37 (1998).
13. ZEMAX Optical Design Program, available from Focus Software Inc., Tucson, AZ.
14. C. C. La Baw: "Integrated filter and detector array for spectral imaging," U.S. Patent No. 5,159,199 (1992).
15. T. G. Chrien, R. O. Green, and M. L. Eastwood, "Accuracy of the spectral and radiometric laboratory calibration of the Airborne Visible/Infrared Imaging Spectrometer (AVIRIS)," in *Imaging Spectroscopy of the Terrestrial Environment*, *Proc. SPIE* **1298**, 37–49 (1990).
16. D. Kavaldjiev and Z. Ninkov, "Subpixel sensitivity map for a charge-coupled device sensor," *Opt. Eng.* **37**, 948–954 (1998).



Pantazis Mouroulis is currently principal optical engineer at the Jet Propulsion Laboratory, California Institute of Technology. Formerly he was an associate professor at the Center for Imaging Science, Rochester Institute of Technology. He received the BS degree in physics from the University of Athens, and the PhD degree in optics from the University of Reading. He has worked and published in areas of optical design, fiber optics, holographic materials, and imaging spectroscopy. He is also coauthor (with J. Macdonald) of *Geometrical Optics and Optical Design*, published by Oxford University Press, and editor of *Visual Instrumentation: Optical Design and Engineering Principles*, published by McGraw-Hill.



Michael M. McKerns is an astrophysics instructor and PhD candidate at the Department of Physics, University of Alabama Birmingham. His dissertation research is in the areas of computational physics and nonlinear optical materials. He received the BS degree in applied physics in 1994 from the University of Notre Dame, and the MS in physics in 1997 from the University of Alabama Birmingham. He has worked as a research assistant for the Conducting Polymers Division, Wright Laboratory, Wright Patterson Air Force Base, and as a research associate for the Imaging and Spectroscopy Systems Technology Section, Jet Propulsion Laboratory, California Institute of Technology.